

A generalized kinetic framework applied to whole-cell catalysis in biofilm flow reactors clarifies performance enhancements

Mir Pouyan Zarabadi,^[a] Manon Couture,^[b, d] Steve J. Charette,^[b, c, d] Jesse Greener*,^[a, e]

Abstract: A common kinetic framework for studies of whole-cell catalysis is vital for understanding and optimizing bioflow reactors. In this work, we demonstrate the applicability of a flow-adapted version of Michaelis-Menten kinetics to a catalytic bacterial biofilm. A three-electrode microfluidic electrochemical flow cell measured increased turnover rates by as much as 50% from a *Geobacter sulfurreducens* biofilm as flow rate was varied. Based on parameters from the applied kinetic framework, flow-induced increases to turnover rate, catalytic efficiency and device reaction capacity could be linked to an increase in catalytic biomass. This study demonstrates that a standardized kinetic framework is critical for quantitative measurements of new living catalytic systems in flow cells and for benchmarking against well-studied catalytic systems such as enzymes.

For centuries, whole-cell biotransformations have been used in the production of food and beverages. More recently, whole-cell biocatalysis has become an active area of research¹ due to its potential for low-cost synthesis of fine chemicals, including chiral molecules and pharmaceuticals,² natural food additives,³ and applications in bioremediation and energy.⁴ Whole-cell biocatalysis benefits from complex multi-enzyme reaction steps, applicability at ambient conditions, and attractive properties such as self-repair and regeneration. It can also be lower in cost compared with extracted enzymes because there is no need for isolation and purification steps and because cells produce their own enzyme co-factors.⁵ Bacterial biofilm are promising for the same reasons, but include other benefits that make them candidates for industrial processes as well.⁶ These include their preference for surface attachment, making them ideal for heterogeneous catalysis and because of their protective self-produced extracellular polymeric matrix, which can mitigate challenges related to toxicity.

Control over substrate concentration and reactor feeding strategy are the most important factors for optimisation of whole-cell biocatalysis.^{7,8} Chemostat bioreactors can impose tunable concentrations against the biofilm and eliminate cyclic nutrient depletion and product accumulation between solution

replenishment in bulk reactors.⁹ However, latency in manipulations of reaction conditions during reaction optimization and fundamental research is a drawback. Microfluidic channels can address this problem because dead space is nearly zero. Combined with strictly laminar flow, microfluidic bioreactors also offer precise control of the shear forces and of diffusion barriers at the biofilm-liquid interface.¹⁰ High surface-area-to-volume ratios result in efficient diffusive mass-transfer between the nutrient solution and the wall-adhered biofilm, even for short contact times at high flow velocities.¹¹ Due to the small volumes used in microfluidic bioreactors, liquid consumption is reduced and thus long-duration studies are possible under a large range of hydrodynamic conditions without the need for frequent refilling of reagent sources. With the proliferation of microfluidic bioanalytical tools for real-time *in situ* measurements of biofilms and their by-products, deeper scientific investigations are possible with better accuracy and repeatability.¹⁰ In this work, we use microfluidic electrochemical flow cells to study whole-cell biofilm electrocatalysis under flow. The kinetic framework used connects whole-cell catalysis in flow systems to traditional Michaelis-Menten kinetics (Eq. 1) between a substrate molecule S and a catalytic bacteria in a biofilm, denoted by E, due to historical relation to enzyme kinetics.^{12,13}



where k_a ($M^{-1}\cdot s^{-1}$) and k'_a (s^{-1}) are the forward and backward rate constants in the first reversible complexation step, and k_{cat} is the catalytic rate constant (s^{-1}) that irreversibly transforms the pre-equilibrated ES complex into the products. The irreversibility of the final transformation is a typical assumption for most biocatalytic systems but should be justified. The Michaelis-Menten constant K_M defines the substrate concentration that results in half-maximal activity. The reader is directed to the supporting information (SI, section 4) for more information. Changes to certain reaction conditions can result in “apparent” or “effective” kinetics, which lead to the apparent Michaelis-Menten constants and efficiency parameters $K_{M(app)}$ and $\epsilon_{(app)}$, respectively. In 1966, Lilly and Hornby developed a framework for enzyme kinetics that accounted for changes to hydrodynamic conditions in flow reactors¹⁴ (Eq. 2).

$$P[S]_i = \frac{C}{Q} + K_{M(app)} \ln(1 - P) \quad (\text{Eq. 2})$$

where $P (= \frac{[S]_i - [S]_f}{[S]_i})$ is the substrate conversion fraction, and $C (= k_{cat}[E]\beta)$ is known as the device reaction capacity, which includes ratio of the reactor void volume to the total reactor volume, β . Assuming that k_{cat} and β are not sensitive to flow, changing C can supply evidence of forced convection through three-dimensional porous systems such as biofilms, a point that is often overlooked for reactive biofilms. Applied to enzyme catalysis, trends in $K_{M(app)}$ are often extrapolated to zero flow $K_{M(app)}^0$ to determine whether enzyme activity is only affected by mass transfer effects $K_M =$

[a] Mirpouyan Zarabadi, Prof. Jesse Greener
Département de Chimie, Faculté des sciences et de génie,
Université Laval, Québec City, QC, Canada.
E-mail: jesse.greener@chm.ulaval.ca

[b, d] Prof. Steve J. Charette, Prof. Manon Couture
Institut de Biologie Intégrative et des Systèmes, Université Laval,
Québec City, QC, Canada.
Département de biochimie, de microbiologie et de bio-informatique,
Faculté des sciences et de génie, Université Laval, Québec City,
QC, Canada.

[c] Prof. Steve J. Charette
Centre de recherche de l'Institut universitaire de cardiologie et de
pneumologie de Québec, Québec City, QC, Canada.

[e] Prof. Jesse Greener
CHU de Québec, centre de recherche, Université Laval, 10 rue de
l'Espinay, Québec, QC, Canada.

Supporting information for this article is given via a link at the end of the document. ((Please delete this text if not appropriate))

$K_{M(\text{app})}^0$ or whether surface immobilization can also change the kinetics.¹⁵⁻¹⁷ For enzymes in their native environment within whole cells or biofilms, it is expected that the K_M value measured during static experiments should be the same as $K_{M(\text{app})}^0$ from flow reactors.

Although Michaelis-Menten kinetics have been applied to whole-cell catalysis, the Lilly-Hornby approach has not, limiting the advancement of whole-cell catalysis in flow reactors. To address this deficiency, the turnover rate ($\frac{d[P]}{dt} = -\frac{d[S]}{dt}$, Eq. S2 in SI) from surface-adhered cells or their biofilms should be measured while accurate control over flow rate and $[S]$ are applied. An electroactive biofilm (EAB) from electrogenic bacteria, such as *Geobacter sulfurreducens* is an excellent choice because it can transfer electrons to an electrode during respiration,¹⁰ enabling direct observations of instantaneous turnover rate using chronoamperometric measurements of electric current. For a monoculture EAB of *G. sulfurreducens* under anaerobic conditions, the turnover rate of an acetate substrate (Ac), namely $\frac{d\text{mol}_{\text{Ac}}}{dt}$ ($\text{mol}_{\text{Ac}} \cdot \text{s}^{-1}$), is calculated from the electrical current I ($\text{C} \cdot \text{s}^{-1}$) using Eq. 3:

$$\frac{d\text{mol}_{\text{Ac}}}{dt} = \frac{I}{8.F} \quad (\text{Eq. 3})$$

where F is Faraday's constant or $F = 9.6485 \times 10^4 \text{ C} \cdot \text{mol}_e^{-1}$, and 8 is the proportionality constant for the number of moles of electrons produced for each mole of Ac oxidized. The irreversible final transformation in Eq. 1 is a good assumption for chronoamperometry experiments on electrode-adhered EABs due to the application of an electrode potential, which can quickly and efficiently conduct electrons away from the reaction site.

In this work, we conducted real-time measurements of the instantaneous turnover rates from EAB of *G. sulfurreducens* bacteria in a microfluidic three-electrode flow cell under controlled reaction conditions. Figure 1a presents the top- and side-view schematics of the device, including the sequential placement of the electrodes. Figure 1b shows a typical scanning electron microscopy image of a mature biofilm on the WE following an experiment. The reader is directed to the SI for additional details on device fabrication, operating conditions, and preparation of *G. sulfurreducens*. The reader is also directed to the SI (Section 5) for a justification that electron transfer kinetics are not rate limiting under different flow conditions. Thus turnover rate can be interpreted substrate conversion via a modified version of Michaelis-Menten kinetics.¹⁸

$$I = I_{\text{max}} \frac{[\text{Ac}]}{K_{M(\text{app})} + [\text{Ac}]} \quad (\text{Eq. 4})$$

where I_{max} is the maximum current output when the substrate $[\text{Ac}]$ is much larger than $K_{M(\text{app})}$.

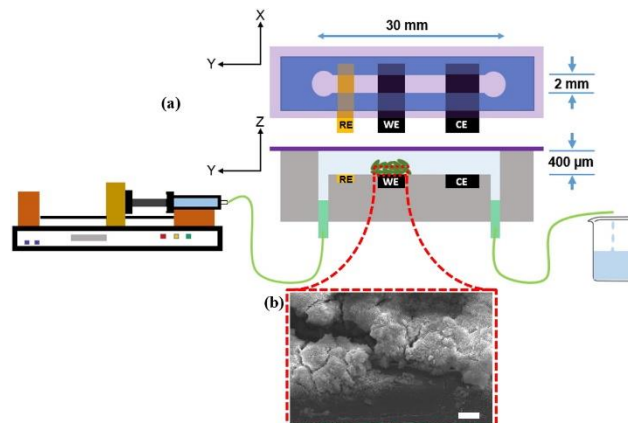


Figure 1 (a) Schematic of the three-electrode electrochemical microfluidic flow channel with channel dimensions 2 mm (w) × 0.4 mm (h) × 30 mm (L). The device was fabricated in PDMS with a glass sealing layer (purple). The top view (x-y plane) through the glass layer (purple) and the side view (y-z plane) show the PDMS channel (grey, or blue as viewed through the glass), the embedded gold reference electrode (RE), and the graphite counter and working electrodes (CE and WE, respectively). The side view shows fluidic connections to the 10 mL gas-tight syringe and pump and the waste and growth of the *G. sulfurreducens* (green) at the WE surface. (b) Scanning electron microscope image of mature *G. sulfurreducens* biofilm (scale bar: 20 μm).

The chronoamperometry data in Figure 2 show peaks in the current I over a background signal of approximately 20 μA as flow pulses ranging from $Q = 0.4$ to 3 $\text{mL} \cdot \text{h}^{-1}$ were applied over a background flow rate of $Q = 0.2 \text{ mL} \cdot \text{h}^{-1}$. The Figure 2 inset plot presents the averaged I vs. Q results from four different measurements on different days. Flow rate of $Q = 3 \text{ mL} \cdot \text{h}^{-1}$ resulted in a 24% increase in current measurements over those acquired at $Q = 0.4 \text{ mL} \cdot \text{h}^{-1}$. Enhancements could not be compared with direct measurements under static conditions ($Q = 0$) because continuous Ac depletion in small microchannel volume around the electrode would prevent stable measurements of current. However, an extrapolation to $Q = 0$ using current values in the linear region from $Q = 0.2$ to $Q = 1 \text{ mL} \cdot \text{h}^{-1}$ gave an estimated zero flow current value of $I = 18.25 \mu\text{A}$ ($3 \text{ A} \cdot \text{m}^{-2}$), which is in the normal range ($1\text{-}10 \text{ A} \cdot \text{m}^{-2}$) for other reported experiments under static conditions. Therefore, we estimated that the turnover rate at 3 $\text{mL} \cdot \text{h}^{-1}$ was more than 50% higher than that under static conditions. Based on the electric current obtained for each flow rate Q , the $[\text{Ac}]$ conversion was calculated for different initial acetate concentrations $[\text{Ac}]_i$ in the range of 0.3 to 10 mM using the formula in Eq. 5:

$$P \cdot [\text{Ac}]_i = [\text{Ac}]_i - [\text{Ac}]_f = \frac{d\text{mol}_{\text{Ac}}}{dt} / Q \quad (\text{Eq. 5})$$

where P is defined for Eq. 2, and $[\text{Ac}]_f$ is the final Ac concentration after biocatalytic oxidation. Figure 3a shows separate plots of the change in $[\text{Ac}]$ as a function of Q for the different applied $[\text{Ac}]_i$. According to Eq. 2, as $[\text{Ac}]_i$ is varied, the plot of $P \cdot [\text{Ac}]_i$ vs. $-\ln(1-P)$ should result in a straight line with slope $-K_{M(\text{app})}$ and intercept C/Q . Such a linear plot was obtained for the five different flow rates used in this work (Figure 3b).

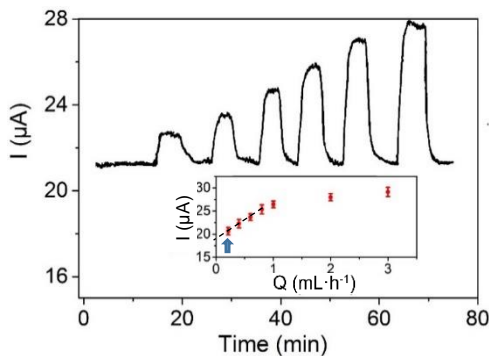


Figure 2 Flow rate modulation from $Q = 0.2 \text{ mL}\cdot\text{h}^{-1}$ (base flow) to elevated values, $Q = 0.4, 0.6, 0.8, 1, 2$ and $3 \text{ mL}\cdot\text{h}^{-1}$ for a 600 h old *G. sulfurreducens* biofilm exposed to $[\text{Ac}] = 10 \text{ mM}$. Inset: average I vs. Q during for a mature biofilm ($> 600 \text{ h}$) conducted 4 times on four consecutive days. Error bars represent standard deviation of averaged measurements. The blue arrow points to data at $Q = 0.2 \text{ mL/h}$ that were acquired from background current measurements, whereas the other values were acquired from peak current values in the main figure. The dashed line extrapolates the linear portion of the inset figure to $Q = 0$ conditions.

Figure 3c shows the values of $K_{M(\text{app})}$ obtained from the slopes in Figure 3b. The trends in $K_{M(\text{app})}$ are discussed after validation of the technique by comparison to the conventional K_M constant from static experiments. First, we extrapolated to $Q = 0$, obtaining $K_{M(\text{app})}^0 = 0.59 \text{ mM}$. Then, direct measurements of K_M were collected from a *G. sulfurreducens* biofilm in a bulk three-electrode system under similar conditions (bacterial age, graphite electrode material and nutrient solution). Electric currents were obtained immediately after stabilization following replacement with a new nutrient solution with a different $[\text{Ac}]$ (SI, Figure S5b). Plotting I vs. $[\text{Ac}]$ produced a standard Michaelis-Menten profile (Figure 3d) and a Lineweaver-Burk plot of $1/I$ vs. $1/[\text{Ac}]$ yielded the expected straight line (Figure 3d inset). A fitting algorithm applied to either curve in Figure 3d yielded a value of $K_M = 0.62 \text{ mM}$. The similarity between K_M and $K_{M(\text{app})}^0$ for the present system also matched the $K_M = 0.60 \text{ mM}$ reported previously for bulk measurements.¹⁸

The implications of reduced $K_{M(\text{app})}$ with increasing Q are examined next. Applied Ac concentrations of 10 mM are considered to lie in the “substrate saturated” regime¹⁹ ($[\text{Ac}] \gg K_M$), and should be described by Eq. S3 (equivalently $I = k_{\text{cat}}[\text{E}]$). Therefore, an increase in either or both of k_{cat} or $[\text{E}]$ could explain the peak I values (Figure 2), which increased by 24% when Q was increased from 0.4 to $3 \text{ mL}\cdot\text{h}^{-1}$. Despite previous suggestions that accelerated turnover under flow could be the result of EAB deacidification,²⁰ a likely route to increases in k_{cat} , pH was recently shown not to change for similar conditions at $[\text{Ac}] = 10 \text{ mM}$.²⁰ Alternatively, flow-induced increases to current might be at least partially related to changes to $[\text{E}]$. In this vein, consider the measurements of device reaction capacity (C), which increased by 19% when increasing flow from $Q = 0.4$ to $Q = 3 \text{ mL}\cdot\text{h}^{-1}$ (SI, Table S1 and Figure S6). Taking into account that C depends only on $[\text{E}]$, k_{cat} , and the physical dimensions implicit in β (Eq. 2), flow-

related increases to C support the likelihood of increases to $[\text{E}]$, assuming that k_{cat} and β remain largely constant. Flow-based increases to $[\text{E}]$ could result from better contact between the acetate molecules and the catalytic bacteria at different strata within the biofilm due to forced convective flow through the porous biofilm, as noted previously for non-electroactive biofilms.^{22, 23} The implication of additional *G. sulfurreducens* bacteria contributing to biocatalysis combined with reduced diffusion barriers around the biofilm at higher flow rates, can be exploited for improvement to device performance in future flow-based bioelectrochemical applications. Global improvements in performance under flow are expressed by increases to (apparent) catalytic efficiency $\epsilon_{(\text{app})} = k_{\text{cat}}/K_{M(\text{app})}$, by replacing K_M with $K_{M(\text{app})}$ in Eq. S4. Notably, increases to $\epsilon_{(\text{app})}$ were calculated to be 19% as Q increased from 0.4 to $3 \text{ mL}\cdot\text{h}^{-1}$, which correspond closely to measured changes to I and C and proposed changes in $[\text{E}]$ for the same flow rate range.

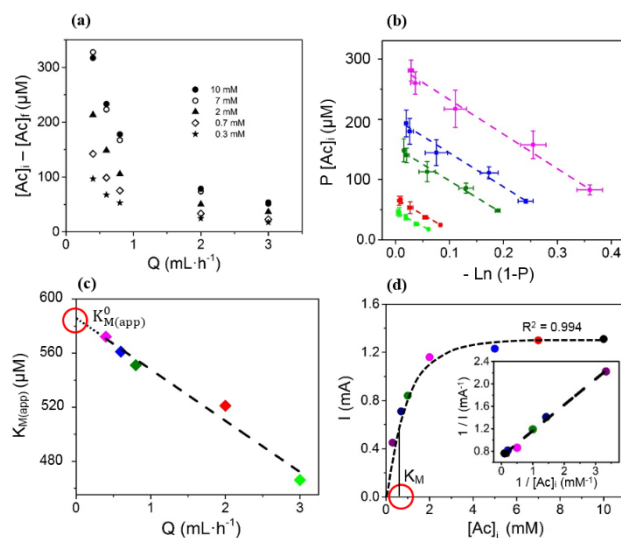


Figure 3 (a) Plots of the concentration of acetate nutrient converted for respiration vs. flow rate as a function of the initial acetate concentration. (b) Plots of $P [\text{Ac}]_i$ vs. $-\text{Ln}(1 - P)$. The modulated flow rates were $Q = 0.4 \text{ mL}\cdot\text{h}^{-1}$ (pink), $0.6 \text{ mL}\cdot\text{h}^{-1}$ (blue), $0.8 \text{ mL}\cdot\text{h}^{-1}$ (dark green), $2 \text{ mL}\cdot\text{h}^{-1}$ (red) and $3 \text{ mL}\cdot\text{h}^{-1}$ (green). (c) Plot of $K_{M(\text{app})}$ vs. Q . The intercept on the vertical axis (red circle) yields a zero-flow $K_{M(\text{app})}$ value ($K_{M(\text{app})}^0$) of 0.59 mM . (d) Current vs. initial acetate concentrations in the bulk experiment for 10 mM (black), 7 mM (red), 5 mM (blue), 2 mM (pink), 1 mM (dark green), 0.7 mM (dark blue) and 0.3 mM (purple). The curve was fitted to Eq. 4 to find $K_{M(\text{app})}$. Inset: The Lineweaver-Burk plot of the reciprocal current output vs. the reciprocal acetate concentration demonstrates the expected linear profile for systems applicable to Michaelis-Menten kinetics.

As applied to the study of *G. sulfurreducens* biofilms, a flow-adapted version of the Michaelis-Menten equation was used for the first time to understand and develop whole-cell catalysis while leveraging the advantages of microfluidic flow cells. Various applications can be envisioned, especially those related to synthetic biology and metabolic engineering in which cells are effectively considered as units of production for valuable products of bulk and fine chemicals.²⁴ In addition, characterization of enzymes within their native (cellular) environment is an important goal in the field of enzymology.²⁵ Our work shows that

measurements of kinetic parameters such as K_M , $\epsilon_{(app)}$, and $[E]$ as a function of flow for whole-cell catalysts is feasible microorganisms immobilized within a microfluidic chamber. Generalization of this approach together with the application of different detection modes for non-electroactive biofilms appears a desirable next step.

Experimental Section

Frozen samples of *Geobacter sulfurreducens* (strain PCA, ATCC 51573), were cultured under controlled temperature and deoxygenated conditions before being injected into the microfluidic electrochemical device. The channel-embedded electrodes were fabricated as shown previously.^{20,26} Graphite was used for both the working (WE) and counter (CE) electrodes and a stable gold (Au) pseudo reference electrode (RE). The device was operated in an anaerobic enclosure with controlled temperature of 23 ± 0.5 °C. Syringe pumps were used for controlled liquid injection while electrochemical measurements were conducted using a potentiationstat for chronoamperometry and cyclic voltammetry.

Acknowledgements

This research was supported by funding from the Natural Sciences and Engineering Research Council, Canada and Sentinelle Nord. J.G. is the recipient of an Early Researcher Award and an AUDACE grant (high risk, high reward) for studies of microbiological systems using microfluidics from the Fonds de recherche du Québec—nature et technologies (FRQNT). The authors wish to thank Molly Gregas for copyedits.

Keywords: whole-cell catalysis • Lilly-Hornby • biofilm flow reactor • electrochemistry • microfluidics

[1] M. M. Domach, *Catal. Lett.* **2015**, *145*, 346-359.
 [2] M. Chartrain, R. Greasham, J. Moore, P. Reider, D. Robinson, B. Buckland, *J. Mol. Catal. B Enzym.* **2001**, *11*, 503-512.
 [3] D. Dasgupta, S. Bandhu, D. K. Adhikari, D. Ghosh, *Microbiol Res.* **2017**, *197*, 9-21.
 [4] C. Santoro, C. Arbizzani, B. Erable, I. Ieropoulos, *J. Power Sources* **2017**, *356*, 225-244.

[5] P. K. Robinson, *Essays Biochem.* **2015**, *59*, 1-41.
 [6] B. Halan, K. Buehler, A. Schmid, *Trends Biotechnol.* **2012**, *30*, 453-465.
 [7] D. Çelik, E. Bayraktar, Ü. Mehmetoğlu, *Biochem Eng J.* **2004**, *17*, 5-13.
 [8] C. Hacka, J. Woodley, M. Lilly, J. Liddell, *Enzyme Microb Technol.* **2000**, *26*, 530-536.
 [9] B. Lin, Y. Tao, *Microb. Cell Fact.* **2017**, *16*, 106.
 [10] M. Pousti, M. P. Zarabadi, M. A. Amirdehi, F. Paquet-Mercier, J. Greener, *Analyst* **2019**, *144*, 68-86.
 [11] M. P. Zarabadi, S.J. Charette, J. Greener, *Submitted*, **2019**.
 [12] D. Villahermosa, A. Corzo, E. Garcia-Robledo, J. M. González, S. Papaspyrou, *PLoS one* **2016**, *11*, e0149096.
 [13] I. Longmuir, *Biochemical Journal* **1954**, *57*, 81.
 [14] M. Lilly, W. Hornby, E. Crook, *Biochem. J.* **1966**, *100*, 718.
 [15] A. A. Halim, N. Szita, F. Baganz, *J. Biotechnol.* **2013**, *168*, 567-575.
 [16] J. Wang, S.-S. Gu, H.-S. Cui, L.-Q. Yang, X.-Y. Wu, *Bioresour Technol.* **2013**, *149*, 367-374.
 [17] G. H. Seong, J. Heo, R. M. Crooks, *Anal. Chem.* **2003**, *75*, 3161-3167.
 [18] X. Zhu, J. C. Tokash, Y. Hong, B. E. Logan, *Bioelectrochemistry* **2013**, *90*, 30-35.
 [19] P. S. Bonanni, G. D. Schrott, L. Robuschi, J. P. Busalmen, *Energy Environ. Sci.* **2012**, *5*, 6188-6195.
 [20] D. Ye, Y. Yang, J. Li, X. Zhu, Q. Liao, B. Deng, R. Chen, *Int. J. Hydrog. Energy* **2013**, *38*, 15710-15715.
 [21] M. P. Zarabadi, S. J. Charette, J. Greener, *ChemElectroChem* **2018**, *5*, 3645-3653.
 [22] D. De Beer, P. Stoodley, Z. Lewandowski, *Water Res.* **1996**, *30*, 2761-2765.
 [23] V. T. Nguyen, E. Morgenroth, H. Eberl, *Water Sci Technol.* **2005**, *52*, 167-172.
 [24] B. Lin, Y. Tao, *Microb Cell Fact.* **2017**, *16*, 106.
 [25] C. Khosla, *Nat. Chem. Biol.* **2015**, *11*, 438.
 [26] M. P. Zarabadi, F. Paquet-Mercier, S. J. Charette, J. Greener, *Langmuir* **2017**, *33*, 2041-2049.